

# Numerical study of hot strongly interacting matter

**P. Petreczky**

Physics Department, Brookhaven National Laboratory, Upton, NY 11973, USA

**Abstract.** I review recent progress in study of strongly interacting matter at high temperatures using Monte-Carlo simulations in lattice QCD.

## 1. Introduction

It is expected that strongly interacting matter undergoes a transition in some temperature interval from hadron gas to deconfined state also called the quark gluon plasma (QGP) [1]. Creating deconfined medium in a laboratory is the subject of the large experimental program at RHIC [2] and LHC [3]. Attempts to study QCD thermodynamics on the lattice go back to the early 80's when lattice calculations in  $SU(2)$  gauge theory provided the first rigorous theoretical evidence for deconfinement [4, 5, 6]. The problem of calculating thermodynamic observables in pure gluonic theory was solved in 1996 [7], while simulations involving dynamical quarks were limited to large quark masses and had no control over the discretization errors [8, 9, 10]. Lattice calculations of QCD thermodynamics with light dynamical quarks remained challenging until recently. During the past six years calculations with light  $u, d$  quarks have been performed using improved staggered fermion actions [11, 12, 13, 14, 15, 16, 17, 18, 19, 20, 21, 22, 24]. There was also progress in lattice QCD calculations at non-zero temperature using Domain Wall and Wilson fermion formulations [25, 26, 27]. However, due to much larger computational costs the corresponding results are far less extensive.

To get reliable predictions from lattice QCD the lattice spacing  $a$  should be sufficiently small relative to the typical QCD scale, i.e.  $\Lambda_{QCD}a \ll 1$ . For staggered fermions, discretization errors go like  $\mathcal{O}((a\Lambda_{QCD})^2)$  but discretization errors due to flavor symmetry breaking turn out to be numerically quite large and dominate the cutoff dependence of thermodynamic quantities at low temperatures. To reduce these errors one has to use improved staggered fermion actions with so-called fat links [28]. At high temperature the dominant discretization errors go like  $(aT)^2$  and therefore could be very large. Thus it is mandatory to use improved discretization schemes, which improve the quark dispersion relation and eliminate these discretization errors. Lattice fermion actions used in numerical calculations typically implement some version of fat links as well as improvement of quark dispersion relation and are referred to as  $p4$ ,  $asqtad$ ,  $HISQ/tree$  and  $stout$ .

In this contribution I am going to discuss lattice QCD calculations on the equation of state, study of deconfinement aspects of the QCD transition, including color screening and fluctuations of conserved charges, determination of the chiral transition temperature, as well as calculations of temporal and spatial meson correlation functions.

## 2. Equation of State

The equation of state has been calculated using different improved staggered fermion actions  $p4$ ,  $asqtad$ ,  $stout$  and  $HISQ/tree$ . In the lattice calculations of the equation of state and many other quantities the temperature is varied by varying the lattice spacing at fixed value of the temporal extent  $N_\tau$ . The temperature  $T$  is given by the lattice spacing and the temporal extent,  $T = 1/(N_\tau a)$ . Therefore taking the continuum limit corresponds to  $N_\tau \rightarrow \infty$  at the fixed physical volume. The calculation of thermodynamic observables proceeds through the calculation of the trace of the energy momentum tensor,  $\epsilon - 3p$ , also known as trace anomaly or interaction measure. This is due to the fact that this quantity can be expressed in terms of expectation values of local gluonic and fermionic operators, (see e.g. Ref. [18]). Different thermodynamic observables can be obtained from the interaction measure through integration of the trace anomaly <sup>1</sup>. The pressure can be written as

$$\frac{p(T)}{T^4} - \frac{p(T_0)}{T_0^4} = \int_{T_0}^T \frac{dT'}{T'^5} (\epsilon - 3p). \quad (1)$$

The lower integration limit  $T_0$  is chosen such that the pressure is exponentially small there. Furthermore, the entropy density can be written as  $s = (\epsilon + p)/T$ . Since the interaction measure is the basic thermodynamic observable in the lattice calculations it is worth to discuss its properties more in detail. In Fig. 1 (left panel) I show the results of calculation with  $p4$  and  $asqtad$  actions using  $N_\tau = 6$  and 8 lattices and light quark masses  $m_l = m_s/10$ , where  $m_s$  is the physical strange quark mass. These calculations correspond in the continuum limit to the pion mass of 220MeV and 260MeV for  $p4$  and  $asqtad$  respectively. The interaction measure shows a rapid rise in the transition region and after reaching a peak at temperatures of about 200MeV decreases. Cutoff effects (i.e.  $N_\tau$  dependence) appears to be the strongest around the peak region and decrease at high temperatures. For temperatures  $T < 270$ MeV calculations with  $p4$  and  $asqtad$  actions have been extended to smaller quark masses,  $m_l = m_s/20$ , that correspond to the pion mass of about 160MeV in the continuum limit [17, 29]. It turns out that the quark mass dependence is negligible for  $m_l < m_s/10$ . Furthermore, for  $asqtad$  action calculations have been extended to  $N_\tau = 12$  lattices [29]. The trace anomaly was calculated with  $HISQ/tree$  action on lattices with temporal extent  $N_\tau = 6$  and 8 and  $m_l = m_s/20$  [29] (corresponding to  $m_\pi = 160$ MeV in the continuum limit). Finally, calculation of the trace anomaly and the equation of state was performed with  $stout$  action using  $N_\tau = 4, 6, 8, 10$  and 12 and physical light quark masses [21]. Using the lattice data from  $N_\tau = 6, 8, 10$  a continuum estimate for different quantities was given [21]. In Fig. 1 (right panel) the results of different lattice calculations of  $\epsilon - 3p$  are summarized corresponding to the pion masses close to the physical value. I also compare the lattice results with the parametrization s95p-v1 of  $\epsilon - 3p$ . This parametrization combines lattice QCD results of Refs. [16, 18] at high temperatures with hadron resonance gas model (HRG) at low temperatures ( $T < 170$ MeV) [31]. At low temperatures there is a fair agreement between the results obtained with  $stout$  action and the results obtained with  $HISQ/tree$  action as well as with  $asqtad$  action for  $N_\tau = 12$ . All these lattice results are slightly above the HRG curve. There is a big difference in the height of the peak in the calculations obtained with  $asqtad$  and  $HISQ/tree$  actions and the continuum estimate for  $stout$  action. The  $p4$  action has large cutoff effects at low temperatures and in the peak region. As the result the  $p4$  results are higher in the peak region and fall below the HRG curve at low temperatures. When cutoff effects in the hadron spectrum are taken into account in the HRG model a good agreement between the  $p4$  data and HRG result can be achieved [31]. Since the dominant cutoff effects of order  $a^2 T^2$  are eliminated, the  $N_\tau$ -dependence is expected to be small for  $p4$ ,  $asqtad$  and  $HISQ/tree$  action at high temperatures. We see that for  $T > 250$ MeV all these lattice

<sup>1</sup> A somewhat different approach was used in Ref. [21]

actions lead to similar results. At temperatures above 350MeV we also see a good agreement with the *stout* results.

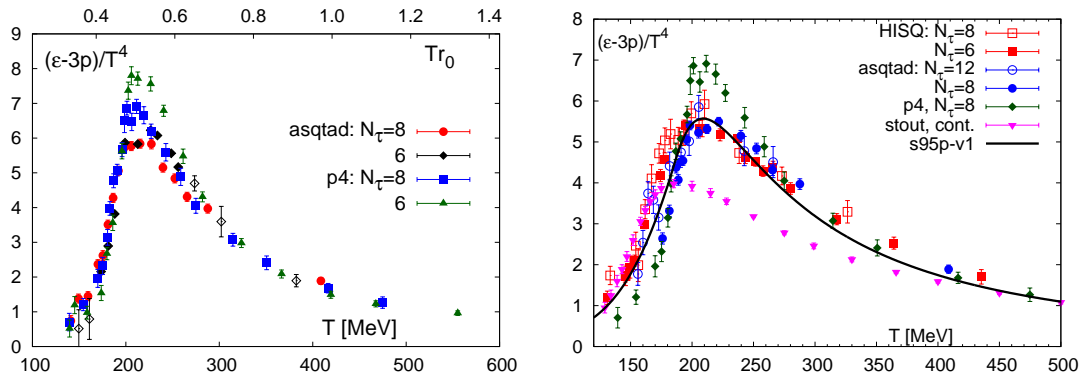


**Figure 1.** The interaction measure calculated with  $m_l = m_s/10$  and *p4* and *asqtad* actions [18] (left) and with  $m_l = m_s/20$  for *p4* action [17] as well as with *HISQ/tree* and *asqtad* actions [29]. Also shown in the figure are the continuum estimates obtained with *stout* action and the parametrization based on hadron resonance gas (HRG) model [31].

The pressure, the energy density and the entropy density are shown in Fig. 2. The energy density shows a rapid rise in the temperature region (170 – 200) MeV and quickly approaches about 90% of the ideal gas value. The pressure rises less rapidly but at the highest temperature it is also only about 15% below the ideal gas value. In the previous calculations with the *p4* action it was found that the pressure and the energy density are below the ideal gas value by about 25% at high temperatures [10]. Possible reason for this larger deviation could be the fact that the quark masses used in this calculation were fixed in units of temperature instead being tuned to give constant meson masses as lattice spacing is decreased. As discussed in Ref. [30] this could reduce the pressure by 10 – 15% at high temperatures. In Fig. 2 I also show the entropy density divided by the corresponding ideal gas value and compare the results of lattice calculations with resummed perturbative calculation [32, 33] as well as with the predictions from AdS/CFT correspondence for the strongly coupled regime [34]. The later is considerably below the lattice results. Note that the pressure, the energy density and the trace anomaly have also been recently discussed in the framework of resummed perturbative calculations which seem to agree with lattice data quite well at high temperatures[35].

The differences between the *stout* action and the *p4* and *asqtad* actions for the trace anomaly translates into the differences in the pressure and the energy density. In particular, the energy density is about 20% below the ideal gas limit for the *stout* action.

### 3. Deconfinement : Fluctuations of conserved charges

Due to the infamous sign problem lattice QCD Monte-Carlo simulations are not possible at non-zero quark chemical potentials. The pressure at non-zero chemical potentials can be evaluated using Taylor expansion. The Taylor expansion can be set up in terms of quark chemical potentials or in terms of chemical potentials corresponding to baryon number  $B$ , electric charge  $Q$  and strangeness  $S$  of hadrons. The expansion coefficients in quark chemical potential  $\chi_{uds}^{jkl}$  and the hadronic ones  $\chi_{BQS}^{jkl}$  are related to each other [36]. While Taylor expansion can be used to study the physics at non-zero baryon density they are interesting on their own right as they are related to the fluctuations of conserved charges. The later are sensitive probes of deconfinement. This is because fluctuation of conserved charges are sensitive to the underlying degrees of freedom which could be hadronic or partonic. Fluctuations of conserved charges have

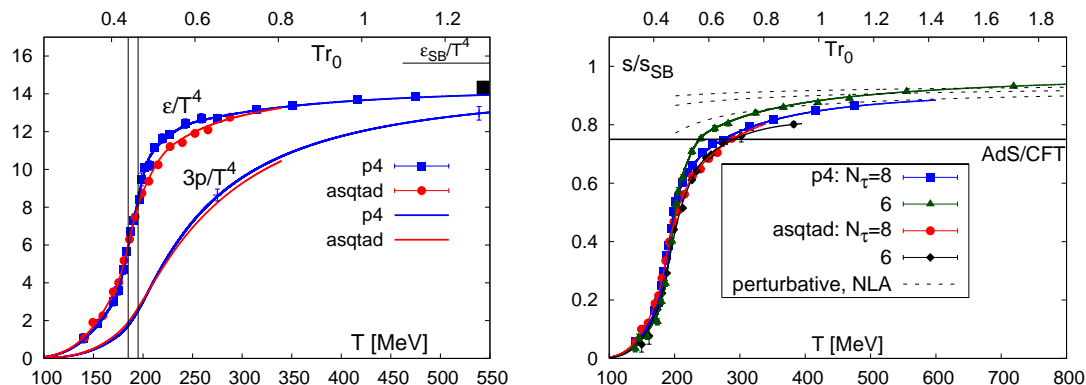


**Figure 2.** The energy density and the pressure as function of the temperature (left), and the entropy density divided by the corresponding ideal gas value (right). The dashed lines in the right panel correspond to the resummed perturbative calculations while the solid black line is the AdS/CFT result.

been studied using different staggered actions [11, 18, 20, 36, 37]. As an example in Fig. 3 I show the quadratic strangeness fluctuation as the function of the temperature. Fluctuations are suppressed at low temperatures because conserved charges are carried by massive strange hadrons (mostly kaons). They are well described by Hadron Resonance Gas (HRG) model at low temperatures. Strangeness fluctuations rapidly grow in the transition region of  $T = (160 - 200)$  MeV as consequence of deconfinement. At temperatures  $T > 250$  MeV strangeness fluctuations are close to unity that corresponds to the massless ideal quark gas. Similar picture can be seen in other fluctuations, in particular for light quark number fluctuation,  $\chi_l$ , which is also shown in Fig. 3. The more rapid rise of  $\chi_l$  in the transition region is presumably a quark mass effect.

The transition from hadronic to quark degrees of freedom can be particularly well seen in the temperature dependence of the Kurtosis, which is the ratio of quartic to quadratic fluctuations. This quantity can be also measured experimentally. In Fig. 4 I show the Kurtosis of the baryon number as a function of the temperature. At low temperatures it is temperature independent and is close to unity in agreement with the prediction of the HRG model. In the transition region it sharply drops from the hadron resonance gas value to the value corresponding to an ideal gas of quarks. Since the fluctuations of conserved charges are so well described by ideal quark gas it is interesting to compare the lattice results for quark number fluctuations with resummed perturbation theory. Quadratic quark number fluctuations are also called quark number susceptibilities and have been calculated in resummed perturbation theory [38, 39, 40]. The comparison of the resummed perturbative results with lattice calculations performed with  $p4$  action [41] for the quark number susceptibility divided by the ideal gas value is shown in Fig. 4. The figure shows a very good agreement between the lattice calculations and resummed perturbative results. Let me finally note that the discretization errors in the lattice calculations of the fluctuations are small at high temperatures when calculated with the  $p4$  action. The same is true for  $asqtad$  action [11, 18].

Fluctuations of conserved charges have also been calculated using gauge/string duality in Refs. [42, 43]. These calculations could reproduce several features of the lattice data.

#### 4. Deconfinement : color screening

One of the most prominent feature of the quark gluon plasma is the presence of chromoelectric (Debye) screening. The easiest way to study chromoelectric screening is to calculate the Polyakov loop. The Polyakov loop is an order parameter for the deconfinement transition in pure gauge

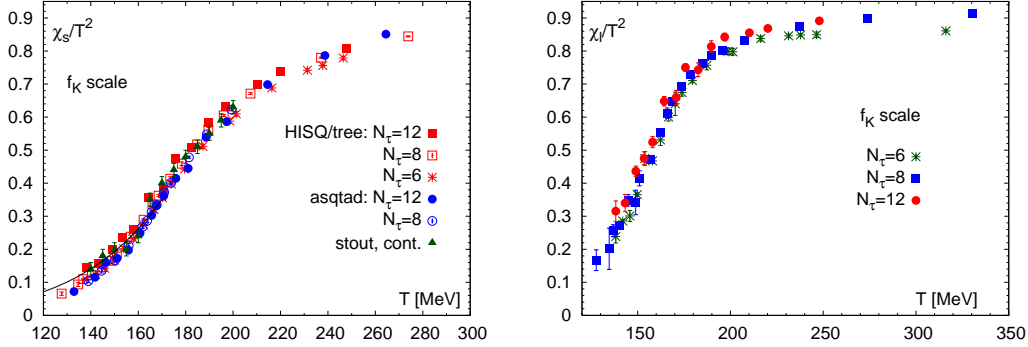


**Figure 3.** Strangeness fluctuation calculated with *asqtad* and *HISQ/tree* actions [24] and compared with the continuum estimate obtained with stout action [20] as well as the prediction of the HRG model shown as a black line (left panel). In the right panel the light quark number fluctuations are shown for *HISQ/tree* action [24].

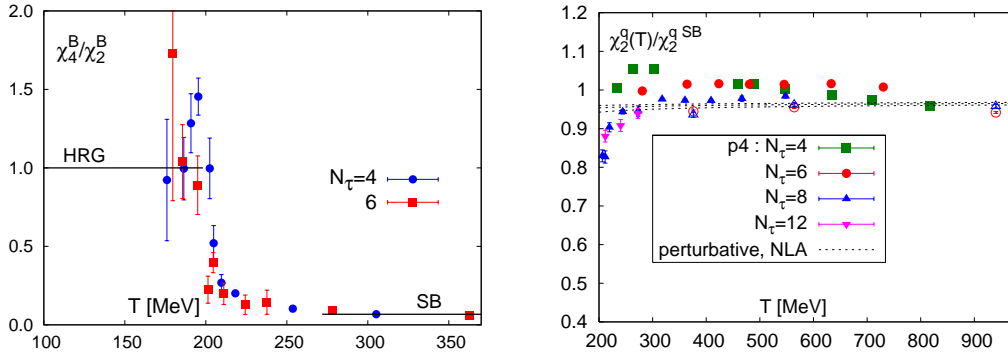


**Figure 4.** The Kurtosis of baryon number (left) and the quark susceptibility compared with resummed perturbative calculations (right). The open symbols on the right plot correspond to *asqtad* results for strange quark number susceptibility [11]. The resummed perturbative results were obtained in next-to-leading approximation (NLA) [39].

theory, which is governed by  $Z(N)$  symmetry. For QCD this symmetry is explicitly broken by dynamical quarks. There is no obvious reason for the Polyakov loop to be sensitive to the singular behavior close to the chiral limit although speculations along these lines have been made [52]. The Polyakov loop is related to the screening properties of the medium and thus to deconfinement. After proper renormalization, the square of the Polyakov loop characterizes the long distance behavior of the static quark anti-quark free energy; it gives the excess in free energy needed to screen two well-separated color charges. The renormalized Polyakov loop has been studied in the past in pure gauge theory [51, 53] as well as in QCD with two [54], three [50] and two plus one flavors [16, 18]. The renormalized Polyakov loop, calculated on lattices with temporal extent  $N_\tau$ , is obtained from the bare Polyakov

$$L_{ren}(T) = z(\beta)^{N_\tau} L_{bare}(\beta) = z(\beta)^{N_\tau} \left\langle \frac{1}{3} \text{Tr} W(\vec{x}) \right\rangle, \quad W(\vec{x}) = \prod_{x_0=0}^{N_\tau-1} U_0(x_0, \vec{x}), \quad (2)$$

where  $U_0 = \exp(igaA_0)$  denotes the temporal gauge link and  $z(\beta)$  is the renormalization constant determined from the  $T = 0$  static potential [24]. The numerical results for the renormalized Polyakov loop for the *HISQ/tree* action are shown in Fig. 5. As one can see from the figure the cutoff ( $N_\tau$ ) dependence of the renormalized Polyakov loop is small. We also compare our results

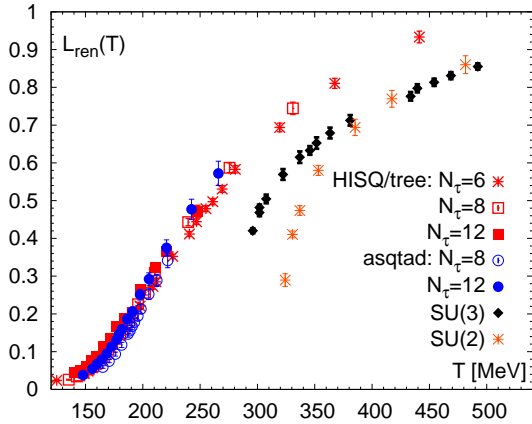


**Figure 5.** The Polyakov loop as function of the temperature in pure gauge theory and 2+1 flavor QCD.

with the continuum extrapolated *stout* results [20] and the corresponding results in pure gauge theory [51, 53]. We find good agreement between our results and the *stout* results. We also see that in the vicinity of the transition temperature the behavior of the renormalized Polyakov loop in QCD and in the pure gauge theory is quite different.

Further insight on chromoelectric screening can be gained by studying the singlet free energy of static quark anti-quark pair (for reviews on this see Ref. [55, 56]), which is expressed in terms of correlation function of temporal Wilson lines in Coulomb gauge

$$\exp(-F_1(r, T)/T) = \frac{1}{3} \text{Tr} \langle W(r) W^\dagger(0) \rangle. \quad (3)$$

Instead of using the Coulomb gauge the singlet free energy can be defined in gauge invariant manner by inserting a spatial gauge connection between the two Wilson lines. Using such definition the singlet free energy has been calculated in  $SU(2)$  gauge theory [57]. It has been found that the singlet free energy calculated this way is close to the result obtained in Coulomb gauge [57]. The singlet free energy turned out to be useful to study quarkonia binding at high temperatures in potential models (see e.g. Refs. [44, 45, 46, 47, 48]). The singlet free energy also appears naturally in the perturbative calculations of the Polyakov loop correlators at short distances [58].

The singlet free energy was recently calculated in QCD with one strange quark and two light quarks with masses corresponding to pion mass of 220MeV on  $16^3 \times 4$  lattices [49]. The numerical results are shown in Fig. 6. At short distances the singlet free energy is temperature independent and coincides with the zero temperature potential. In purely gluonic theory the free energy grows linearly with the separation between the heavy quark and anti-quark in the confined phase. In presence of dynamical quarks the free energy is saturated at some finite value at distances of about 1 fm due to string breaking [55, 50, 54]. This is also seen in Fig. 6. Above the deconfinement temperature the singlet free energy is exponentially screened at sufficiently large distances [51, 53] with the screening mass proportional to the temperature, i.e.

$$F_1(r, T) = F_\infty(T) - \frac{4}{3} \frac{g^2(T)}{4\pi r} \exp(-m_D(T)r), \quad m_D \sim T. \quad (4)$$

Therefore in Fig. 6 I also show the combination  $F_1(r, T) - F_\infty(T)$  as a function of  $rT$ . As one can see from the figure this function shows an exponential fall-off at distances  $rT > 0.8$ . The fact that the slope is the same for all temperatures means that  $m_D \sim T$ , as expected.

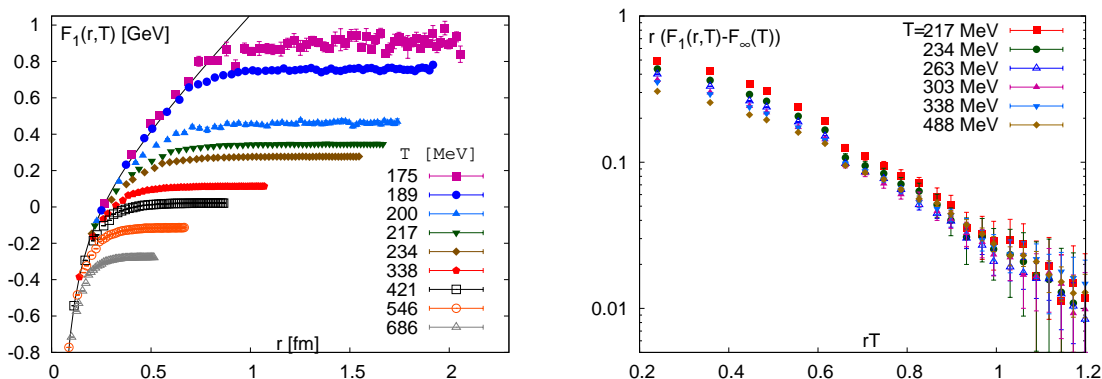


**Figure 6.** The singlet free energy  $F_1(r, T)$  calculated in Coulomb gauge on  $16^3 \times 4$  lattices (left) and the combination  $F_1(r, T) - F_\infty(T)$  as function of  $rT$  (right). The solid black line is the parametrization of the zero temperature potential.

Let me finally note that contrary to the electro magnetic plasma the static chromomagnetic fields are screened in QGP. This is due to the fact that unlike photons gluons interact with each other (the stress tensor is non-linear in QCD). Magnetic screening is non-perturbative, i.e. it does not appear at any finite order of perturbation theory. In lattice calculations chromomagnetic screening is studied either in terms of spatial Wilson loops [59] or in terms of spatial gluon propagators [60, 61, 62]. The numerical results obtained so far show that the length scale related to magnetic screening is larger than the one related to electric screening.

## 5. Chiral transition

The Lagrangian of QCD has an approximate  $SU_A(3)$  chiral symmetry. This symmetry is broken in the vacuum. The chiral symmetry breaking is signaled by non-zero expectation value of the quark or chiral condensate,  $\langle \bar{\psi}\psi \rangle \neq 0$  in the massless limit. This symmetry is expected to be restored at high temperatures and the quark condensate vanishes. There is an explicit breaking of the chiral symmetry by the small value of  $u, d$  and  $s$  quark masses. While due to the relatively large strange quark mass ( $m_s \simeq 100$  MeV)  $SU_A(3)$  may not be a very good symmetry its subgroup  $SU_A(2)$  remains a very good symmetry and is relevant for the discussion of the finite temperature transition in QCD. If the relevant symmetry is  $SU_A(2)$  the chiral transition is expected to be second order for massless light ( $u$  and  $d$ ) quarks belonging to the  $O(4)$  universality class. Recent calculations with  $p4$  action support this picture [63]. This also means that for non-zero light quark masses the transition must be a crossover. The latter fact seems to be supported by calculations in Ref. [64]. The  $U_A(1)$  symmetry is explicitly broken in the vacuum by the anomaly but it is expected to be effectively restored at high temperatures as non-perturbative vacuum fluctuations responsible for its breaking are suppressed at high temperatures. If the  $U_A(1)$  symmetry is restored at the same temperature as the  $SU_A(2)$  symmetry the transition could be first order [65]. Recent calculations with staggered as well as with domain wall fermions suggest that  $U_A(1)$  symmetry gets restored at temperature that is significantly higher than the chiral transition temperature [25, 66].

For massless quark the chiral condensate vanishes at the critical temperature  $T_c^0$  and is the order parameter. Therefore in the lattice studies one calculates the chiral condensate and its derivative with respect to the quark mass called the chiral susceptibility. For the staggered fermion formulation most commonly used in the lattice calculations these quantities can be

written as follows:

$$\langle \bar{\psi}\psi \rangle_{q,x} = \frac{1}{4} \frac{1}{N_\sigma^3 N_\tau} \text{Tr} \langle D_q^{-1} \rangle, \quad (5)$$

$$\chi_{m,q}(T) = n_f \frac{\partial \langle \bar{\psi}\psi \rangle_{q,\tau}}{\partial m_l} = \chi_{q,disc} + \chi_{q,con} \quad q = l, s, \quad (6)$$

where the subscript  $x = \tau$  and  $x = 0$  will denote the expectation value at finite and zero temperature, respectively. Furthermore,  $D_q = m_q \cdot 1 + D$  is the fermion matrix in the canonical normalization and  $n_f = 2$  and  $1$  for light and strange quark. In Eq. (6) we made explicit that chiral susceptibility is the sum of connected and disconnected Feynman diagrams. The disconnected and connected contributions can be written as

$$\chi_{q,disc} = \frac{n_f^2}{16N_\sigma^3 N_\tau} \left\{ \langle (\text{Tr} D_q^{-1})^2 \rangle - \langle \text{Tr} D_q^{-1} \rangle^2 \right\}, \quad (7)$$

$$\chi_{q,con} = -\frac{n_f}{4} \text{Tr} \sum_x \langle D_q^{-1}(x,0) D_q^{-1}(0,x) \rangle, \quad q = l, s. \quad (8)$$

The disconnected part of the light quark susceptibility describes the fluctuations in the light quark condensate and is directly analogous to the fluctuations in the order parameter of an  $O(N)$  spin model. The second term ( $\chi_{q,con}$ ) arises from the explicit quark mass dependence of the chiral condensate and is the expectation value of the volume integral of the correlation function of the (isovector) scalar operator  $\bar{\psi}\psi$ . Let me note that in the massless limit only  $\chi_{l,disc}$  diverges.

### 5.1. The temperature dependence of the chiral condensate

The chiral condensate needs a multiplicative, and also an additive renormalization if the quark mass is non-zero. Therefore the subtracted chiral condensate is considered

$$\Delta_{l,s}(T) = \frac{\langle \bar{\psi}\psi \rangle_{l,\tau} - \frac{m_l}{m_s} \langle \bar{\psi}\psi \rangle_{s,\tau}}{\langle \bar{\psi}\psi \rangle_{l,0} - \frac{m_l}{m_s} \langle \bar{\psi}\psi \rangle_{s,0}}. \quad (9)$$

In Fig. 7 I show the results for  $\Delta_{l,s}$  calculated with *HISQ/tree* action and compared to the renormalized Polyakov loop and light quark number fluctuation discussed in relation to the deconfining transition. Interestingly the rapid decrease in the subtracted chiral condensate happens at temperatures that are smaller than the temperatures where the Polyakov loop rises rapidly. On the other hand the rapid change in  $\chi_l$  and  $\Delta_{l,s}$  happen roughly in the same temperature region.

Another way to get rid of the multiplicative and additive renormalization is to subtract the zero temperature condensate and multiply the difference by the strange quark mass, i.e. consider the following quantity

$$\Delta_q^R = d + n_f m_s r_1^4 (\langle \bar{\psi}\psi \rangle_{q,\tau} - \langle \bar{\psi}\psi \rangle_{q,0}) \quad q = l, s. \quad (10)$$

As before,  $n_f = 2$  for light quarks and  $n_f = 1$  for strange quarks, while  $d$  is a normalization constant. The factor  $r_1^4$  was introduced to make the combination dimensionless. Here  $r_1$  is the scale parameter defined from the zero temperature static potential [24]. It is convenient to choose the normalization constant to be the light quark condensate for  $m_l = 0$  multiplied by  $m_s r_1^4$ . In Fig. 8 the renormalized quark condensate is shown as function of temperature for *HISQ/tree* and *stout* actions. We see a crossover behavior for temperature of (150 – 160) MeV, where  $\Delta_q^R$  drops by 50%. The difference between the *stout* and *HISQ/tree* results is a quark



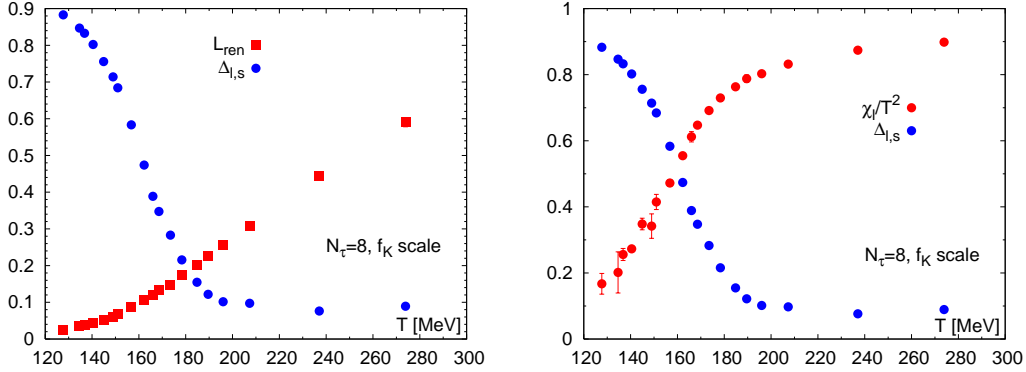


**Figure 7.** The subtracted chiral condensate calculated with *HISQ/tree* action on  $N_\tau = 8$  lattice and compared to the renormalized Polyakov loop (left) and light quark number fluctuation (right).

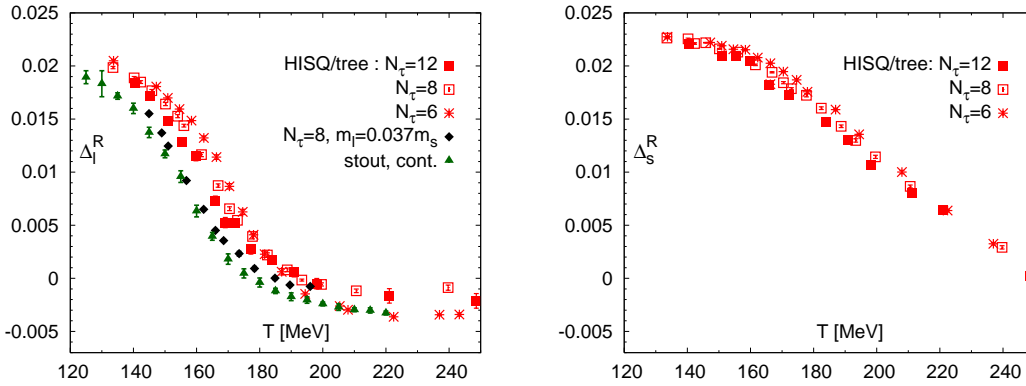


**Figure 8.** The renormalized chiral condensate  $\Delta_l^R$  for the *HISQ/tree* action with  $m_l/m_s = 0.05$  is compared to the *stout* data. In the right panel, we show the renormalized strange quark condensate  $\Delta_s^R$  for the *HISQ/tree* action.

mass effect. Calculations for *HISQ/tree* action were performed for  $m_\pi = 160$  MeV, while the *stout* calculations were done for the physical quark mass. For a direct comparison with *stout* results, we extrapolate the *HISQ/tree* data in the light quark mass and also take care of the residual cutoff dependence in the *HISQ/tree* data. This was done in Ref. [24] and the results are shown in the figure as black diamonds demonstrating a good agreement between *HISQ/tree* and *stout* results. Contrary to  $\Delta_l^R$  the renormalized strange quark condensate  $\Delta_s^R$  shows only a gradual decrease over a wide temperature interval dropping by 50% only at significantly higher temperatures of about 190 MeV.

### 5.2. The chiral susceptibility

For a true chiral phase transition the chiral susceptibility diverges at the transition temperature. For physical value of the quark masses we expect to see a peak in the chiral susceptibility at certain temperature that defines the crossover temperature. The chiral susceptibility also needs a multiplicative and additive renormalization Therefore the following quantity is considered

$$\frac{\chi_R(T)}{T^4} = \frac{m_s^2}{T^4} (\chi_{m,l}(T) - \chi_{m,l}(T=0)). \quad (11)$$

The numerical results for this quantity were presented in Ref. [14] for *stout* action and in Ref. [24] for the *HISQ/tree* action. It was shown that the results of the two calculations agree quite well up to small quark mass effects [24]<sup>2</sup>.

### 5.3. $O(N)$ scaling and the transition temperature

In the vicinity of the chiral phase transition, the free energy density may be expressed as a sum of a singular and a regular part,

$$f = -\frac{T}{V} \ln Z \equiv f_{sing}(t, h) + f_{reg}(T, m_l, m_s). \quad (12)$$

Here  $t$  and  $h$  are dimensionless couplings that control deviations from criticality. They are related to the temperature  $T$  and the light quark mass  $m_l$  as

$$t = \frac{1}{t_0} \frac{T - T_c^0}{T_c^0}, \quad h = \frac{1}{h_0} H, \quad H = \frac{m_l}{m_s}, \quad (13)$$

where  $T_c^0$  denotes the chiral phase transition temperature, *i.e.*, the transition temperature at  $H = 0$ . The scaling variables  $t, h$  are normalized by two parameters  $t_0$  and  $h_0$ , which are unique to QCD and similar to the low energy constants in the chiral Lagrangian. These need to be determined together with  $T_c^0$ . In the continuum limit, all three parameters are uniquely defined, but depend on the value of the strange quark mass.

The singular contribution to the free energy density is a homogeneous function of the two variables  $t$  and  $h$ . Its invariance under scale transformations can be used to express it in terms of a single scaling variable

$$z = t/h^{1/\beta\delta} = \frac{1}{t_0} \frac{T - T_c^0}{T_c^0} \left( \frac{h_0}{H} \right)^{1/\beta\delta} = \frac{1}{z_0} \frac{T - T_c^0}{T_c^0} \left( \frac{1}{H} \right)^{1/\beta\delta} \quad (14)$$

where  $\beta$  and  $\delta$  are the critical exponents of the  $O(N)$  universality class and  $z_0 = t_0/h_0^{1/\beta\delta}$ . Thus, the dimensionless free energy density  $\tilde{f} \equiv f/T^4$  can be written as

$$\tilde{f}(T, m_l, m_s) = h^{1+1/\delta} f_f(z) + f_{reg}(T, H, m_s), \quad (15)$$

where  $f_f$  is the universal scaling function and the regular term  $f_{reg}$  gives rise to scaling violations. This regular term can be expanded in a Taylor series around  $(t, h) = (0, 0)$ .

It should be noted that the reduced temperature  $t$  may depend on other couplings in the QCD Lagrangian which do not explicitly break chiral symmetry. In particular, it depends on light and strange quark chemical potentials  $\mu_q$ , which in leading order enter only quadratically,

$$t = \frac{1}{t_0} \left( \frac{T - T_c^0}{T_c^0} + \sum_{q=l,s} \kappa_q \left( \frac{\mu_q}{T} \right)^2 + \kappa_{ls} \frac{\mu_l \mu_s}{T^2} \right). \quad (16)$$

The transition temperature can be defined as peaks in susceptibilities (response functions) that are second derivatives of the free energy density with respect to relevant parameters. Since there are two relevant parameters we can define three susceptibilities:

$$\chi_{m,l} = \frac{\partial^2 \tilde{f}}{\partial m_l^2}, \quad \chi_{t,l} = \frac{\partial^2 \tilde{f}}{\partial t \partial m_l}, \quad \chi_{t,t} = \frac{\partial^2 \tilde{f}}{\partial t^2}. \quad (17)$$

<sup>2</sup> In Ref. [14] the light quark mass was used instead of  $m_s$  in Eq. (11). In the comparison with was taken into account [24].

Thus three different pseudo-critical temperatures  $T_{m,l}$ ,  $T_{t,l}$  and  $T_{t,t}$  can be defined. In the vicinity of the critical point the behavior of these susceptibilities is controlled by three universal scaling function that can be derived from  $f_f$ . In the chiral limit  $T_{m,l} = T_{t,l} = T_{t,t} = T_c^0$ . There is, however, an additional complication for  $O(N)$  universality class: while  $\chi_{m,l}$  and  $\chi_{t,l}$  diverge at the critical point for  $m_l \rightarrow 0$

$$\chi_{m,l} \sim m_l^{1/\delta-1}, \quad \chi_{t,l} \sim m_l^{(\beta-1)/\beta\delta}, \quad (18)$$

$\chi_{t,t}$  is finite because  $\alpha < 0$  for  $O(N)$  models ( $\chi_{t,t} \sim |t|^{-\alpha}$ ). Therefore, one has to consider the third derivative of  $\tilde{f}$  with respect to  $t$ :

$$\chi_{t,t,t} = \frac{\partial^3 \tilde{f}}{\partial t^3}. \quad (19)$$

In the vicinity of the critical point the derivatives with respect to  $t$  can be estimated by taking the derivatives with respect to  $\mu_l^2$ , i.e. the response functions  $\chi_{t,l}$  and  $\chi_{t,t,t}$  are identical to the first Taylor expansion coefficient of the quark condensate and the sixth order expansion coefficient to the pressure, respectively. The former controls the curvature of the transition temperature as function of the quark chemical potential  $\mu_q$  and was studied for  $p4$  action using  $N_\tau = 4$  and 8 lattices [67]. The later corresponds to the sixth order quark number fluctuation which is related to the deconfinement aspects of the transition. The fact that this quantity is sensitive to the chiral dynamics points to a relation between deconfining and chiral aspects of the transition. In the following I discuss the determination of the transition temperature defined as peak position of  $\chi_{m,l}$ , i.e.  $T_c = T_{m,l}$ .

#### 5.4. Determination of the transition temperature

The  $O(N)$  scaling described in the above subsection can be used to determine the pseudo-critical temperature of the chiral transition. For the study of the  $O(N)$  scaling it is convenient to consider the dimensionless order parameter

$$M_b = m_s \frac{\langle \bar{\psi}\psi \rangle_l}{T^4}. \quad (20)$$

The subscript "b" refers to the fact that this is a bare quantity since the additive UV divergence is not removed. From the point of view of the scaling analysis this divergent term is just a regular contribution. For sufficiently small quark mass and in the vicinity of the transition region we can write

$$M_b(T, H) = h^{1/\delta} f_G(t/h^{1/\beta\delta}) + f_{M,reg}(T, H). \quad (21)$$

Here  $f_G(z)$  is the scaling function related to  $f_f$  and was calculated for  $O(2)$  and  $O(4)$  spin models [68, 69, 70]. The regular contribution can be parametrized as [24]

$$\begin{aligned} f_{M,reg}(T, H) &= a_t(T)H \\ &= \left( a_0 + a_1 \frac{T - T_c^0}{T_c^0} + a_2 \left( \frac{T - T_c^0}{T_c^0} \right)^2 \right) H. \end{aligned} \quad (22)$$

Then we have the following behavior for the light chiral susceptibility

$$\begin{aligned} \frac{\chi_{m,l}}{T^2} &= \frac{T^2}{m_s^2} \left( \frac{1}{h_0} h^{1/\delta-1} f_\chi(z) + \frac{\partial f_{M,reg}(T, H)}{\partial H} \right), \\ \text{with } f_\chi(z) &= \frac{1}{\delta} [f_G(z) - \frac{z}{\beta} f'_G(z)]. \end{aligned} \quad (23)$$

One then performs a simultaneous fit to the lattice data for  $M_b$  and  $\chi_{m,l}$  treating  $T_c^0, t_0, h_0, a_0, a_1$  and  $a_2$  as fit parameters [24]. This gives a good description of the quark mass and temperature dependence of  $\chi_{m,l}$  and allows to determine accurately the peak position in  $\chi_{m,l}$ . As an example in Fig. 1 show the  $O(4)$  scaling fits for  $N_\tau = 8$  lattice data obtained with *HISQ/tree* action. The scaling fit works quite well. Similar results have been obtained for  $N_\tau = 6$  and 12 as well as for *asqtad* action on  $N_\tau = 8$  and 12 lattices [24]. Furthermore, scaling fits have been performed assuming  $O(2)$  universality class. The quality of these fits were similar to the  $O(4)$  ones and the resulting transition temperatures turned out to be the same within statistical errors [24]. Having determined  $T_c$  for *HISQ/tree* and *asqtad* action for each  $N_\tau$  a combined continuum extrapolation was performed using different assumption about the  $N_\tau$  dependence. of  $T_c$  This analysis gave [24]:

$$T_c = (159 \pm 9)\text{MeV}. \quad (24)$$

The analysis also demonstrated that *HISQ/tree* and *asqtad* action give consistent results in the continuum limit. The Budapest-Wuppertal collaboration found  $T_c = 147(2)(3)\text{MeV}$ ,  $157(3)(3)\text{MeV}$  and  $155(3)(3)\text{MeV}$  defined as peak position in  $\chi_R$ , inflection points in  $\Delta_{l,s}$  and  $\Delta_l^R$  respectively [20]. These agree with the above value within errors.

## 6. Temporal meson correlators and spectral functions

Information on hadron properties at finite temperature as well as the transport coefficients are encoded in different spectral functions. In particular the fate of different quarkonium states in QGP can be studied by calculating the corresponding quarkonium spectral functions (for a recent review see Ref. [56]). On the lattice we can calculate correlation function in Euclidean time. This is related to the spectral function via integral relation

$$G(\tau, T) = \int_0^\infty d\omega \sigma(\omega, T) K(\tau, \omega, T), \quad K(\tau, \omega, T) = \frac{\cosh(\omega(\tau - 1/2T))}{\sinh(\omega/2T)}. \quad (25)$$

Given the data on the Euclidean meson correlator  $G(\tau, T)$  the meson spectral function can be calculated using the Maximum Entropy Method (MEM) [72]. For charmonium this was done by using correlators calculated on isotropic lattices [73, 74] as well as anisotropic lattices [75, 76, 77] in the quenched approximation. It has been found that quarkonium correlation

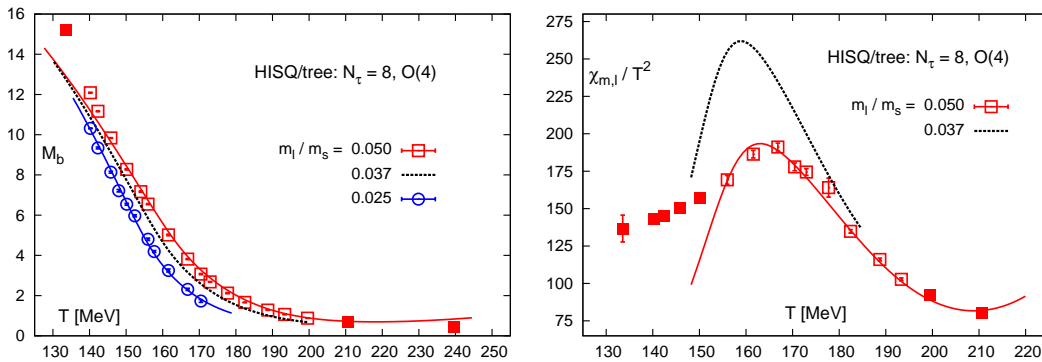


**Figure 9.** Scaling fits and data for the chiral condensate  $M_b$  calculated with the *HISQ/tree* action on lattices with temporal extent  $N_\tau = 8$  (left) and the chiral susceptibility  $\chi_{m,l}$  (right). The data for  $M_b$  at  $m_l/m_s = 0.025$  and for  $M_b$  and  $\chi_{m,l}$  at  $m_l/m_s = 0.05$  are fit simultaneously using the  $O(4)$  scaling Ansatz. The points used in the scaling fits are plotted using open symbols. The dotted lines give the data scaled to the physical quark masses.

function in Euclidean time show only very small temperature dependence [74, 77]. In other channels, namely the vector, scalar and axial-vector channels stronger temperature dependence was found [74, 77]. The spectral functions in the pseudo-scalar and vector channels reconstructed from MEM show peak structures which may be interpreted as a ground state peak [74, 75, 76]. Together with the weak temperature dependence of the correlation functions this was taken as strong indication that the 1S charmonia ( $\eta_c$  and  $J/\psi$ ) survive in the deconfined phase to temperatures as high as  $1.6T_c$  [74, 75, 76]. A detailed study of the systematic effects show, however, that the reconstruction of the charmonium spectral function is not reliable at high temperatures [77], in particular the presence of peaks corresponding to bound states cannot be reliably established. Presence of large cutoff effects at high frequencies also complicates the analysis [80]. The only statement that can be made is that the spectral function does not show significant changes within the errors of the calculations. Recently quarkonium spectral functions have been studied using potential models and lattice data for the singlet free energy of static quark anti-quark pair [46, 47, 48]. These calculations show that all charmonium states are dissolved at temperatures smaller than  $1.2T_c$ , but the Euclidean correlators do not show significant changes and are in fairly good agreement with available lattice data both for charmonium [74, 77] and bottomonium [77, 78]. This is due to the fact that even in absence of bound states quarkonium spectral functions show significant enhancement in the threshold region [45]. Therefore previous statements about quarkonia survival at high temperatures have to be revisited. Exploratory calculations of the charmonium correlators and spectral functions in 2-flavor QCD have been reported in Ref. [79] and the qualitative behavior of the correlation functions was found to be similar.

The large enhancement of the quarkonium correlators above deconfinement in the scalar and axial-vector channel can be understood in terms of the zero mode contribution [45, 81] and not due to the dissolution of the  $1P$  states as previously thought. Similar, though smaller in magnitude, enhancement of quarkonium correlators due to zero mode is seen also in the vector channel [77]. Here it is related to heavy quark transport [44, 82]. Due to the heavy quark mass the Euclidean correlators for heavy quarkonium can be decomposed into a high and low energy part  $G(\tau, T) = G_{\text{low}}(\tau, T) + G_{\text{high}}(\tau, T)$ . The area under the peak in the spectral functions at zero energy  $\omega \simeq 0$  giving the zero mode contribution to the Euclidean correlator is proportional to some susceptibility,  $G_{\text{low}}^i(\tau, T) \simeq T\chi^i(T)$ , which have been calculated on the lattice in Ref. [83]. It is natural to ask whether the generalized susceptibilities can be described by a quasi-particle model. The generalized susceptibilities have been calculated in Ref. [84] in the free theory. Replacing the bare quark mass entering in the expression of the generalized susceptibilities by an effective temperature dependent masses one can describe the zero mode contribution very well in all channels [83].

While temporal correlators are not sensitive to the change in the spectral functions spatial quarkonium correlation functions could be more sensitive to this. Recent lattice calculations show indication for significant change in spatial charmonium correlators above deconfinement[85].

The analysis of the meson spectral functions was also performed in the light quark sector [86, 87, 89, 88]. Somewhat surprisingly this analysis revealed peak structures in the deconfined phase which are difficult to interpret. Most likely the peak structures are artifacts of the MEM analysis. The new analysis of the vector spectral function performed on fine lattices and using several lattice spacings did not show any evidence for such structures [90]. Furthermore, the same analysis revealed the expected transport peak at low frequencies and estimated the electric conductivity to be [90]:

$$1/3 < \frac{\sigma}{C_{em}T} < 1, \quad C_{em} = e^2 \sum_q Q_q^2. \quad (26)$$

## 7. Conclusions

Recently significant progress has been made in lattice QCD calculations at non-zero temperature. Chiral and deconfining aspects of the QCD transition have been studied using improved staggered quark formulation allowing to control discretization effects. It has been shown that in the continuum limit different discretization schemes give consistent results. In particular, agreement has been reached on the value of the chiral transition temperature. There is still disagreement in the lattice calculation of the equation of state. Finally significant progress has been made in lattice calculations of meson spectral functions that encode in-medium meson properties and transport coefficients.

## Acknowledgments

This work was supported by U.S. Department of Energy under Contract No. DE-AC02-98CH10886. Computations have been performed using the USQCD resources on clusters at Fermilab and JLab and the QCDOC supercomputers at BNL, as well as the BlueGene/L at the New York Center for Computational Sciences (NYCCS).

- [1] D. Gross, R. Pisarski, L. Yaffe, *Rev. Mod. Phys.* **53**, 43 (1981)
- [2] B. Müller and J. Nagle, *Ann. Rev. Nucl. Part. Sci.* **56**, 93 (2006)
- [3] U. Wiedemann, *Nucl. Phys. A*, **830**, 74c (2009)
- [4] J. Kuti, J. Polónyi and K. Szlachányi, *Phys. Lett. B* **98** (1981) 199;
- [5] L. D. McLerran and B. Svetitsky, *Phys. Rev. D* **24** (1981) 450;
- [6] J. Engels, F. Karsch, H. Satz and I. Montvay, *Phys. Lett. B* **101** (1981) 89.
- [7] G. Boyd *et al.*, *Nucl. Phys. B* **469**, 419 (1996)
- [8] C. W. Bernard *et al.*, [MILC Collaboration], *Phys. Rev. D* **55** (1997) 6861
- [9] A. Ali Khan *et al.*, [CP-PACS Collaboration], *Phys. Rev. D* **64** (2001) 074510
- [10] F. Karsch, E. Laermann and A. Peikert, *Phys. Lett. B* **478** (2000) 447;
- [11] C. Bernard *et al.* [MILC Collaboration], *Phys. Rev. D* **71**, 034504 (2005)
- [12] Y. Aoki *et al.* *JHEP* **0601**, 089 (2006)
- [13] M. Cheng *et al.*, *Phys. Rev. D* **74**, 054507 (2006)
- [14] Y. Aoki *et al.*, *Phys. Lett. B* **643** (2006) 46 [arXiv:hep-lat/0609068].
- [15] C. Bernard *et al.*, *Phys. Rev. D* **75** (2007) 094505
- [16] M. Cheng *et al.*, *Phys. Rev. D* **77** (2008) 014511
- [17] M. Cheng *et al.*, *Phys. Rev. D* **81**, 054504 (2010)
- [18] A. Bazavov *et al.*, *Phys. Rev. D* **80** (2009), 014504
- [19] Y. Aoki, *et al.*, *JHEP* **0906** (2009) 088
- [20] S. Borsanyi *et al.* [Wuppertal-Budapest Collaboration], *JHEP* **1009**, 073 (2010)
- [21] S. Borsanyi *et al.*, *JHEP* **1011**, 077 (2010)
- [22] A. Bazavov and P. Petreczky [HotQCD collaboration], *J. Phys. Conf. Ser.* **230**, 012014 (2010);
- [23] A. Bazavov and P. Petreczky [HotQCD Collaboration], *PoS LAT2009*, 163 (2009)
- [24] A. Bazavov *et al.*, arXiv:1111.1710 [hep-lat].
- [25] P. Hegde, arXiv:1112.0364v1 [hep-lat]
- [26] S. Borsanyi *et al.*, arXiv:1111.3500 [hep-lat].
- [27] T. Umeda *et al.* [WHOT-QCD Collaboration], *PoS LATTICE 2010*, 218 (2010); arXiv:1101.5582 [hep-lat].
- [28] K. Orginos, D. Toussaint and R. L. Sugar [MILC Collaboration], *Phys. Rev. D* **60** (1999) 054503
- [29] A. Bazavov *et al.* [for the HotQCD Collaboration], *PoS LATTICE 2010*, 169 (2010); W. Soldner [HotQCD Collaboration], *PoS LATTICE 2010*, 215 (2010)
- [30] F. Csikor, *et al.*, *JHEP* **0405** (2004) 046
- [31] P. Huovinen and P. Petreczky, *Nucl. Phys. A* **837**, 26 (2010)
- [32] J. P. Blaizot, E. Iancu and A. Rebhan, *Phys. Rev. Lett.* **83** (1999) 2906;
- [33] J. P. Blaizot, E. Iancu and A. Rebhan, *Phys. Rev. D* **63** (2001) 065003
- [34] S.S. Gubser, I.R. Klebanov and I.I Tseytlin, *Nucl. Phys. B* **534** (1998) 202
- [35] J. O. Andersen, L. E. Leganger, M. Strickland and N. Su, arXiv:1009.4644 [hep-ph].
- [36] M. Cheng *et al.*, *Phys. Rev. D* **79** (2009) 074505
- [37] S. Borsanyi *et al.* [Wuppertal-Budapest Collaboration], *J. Phys. G G* **38**, 124060 (2011)
- [38] J. P. Blaizot, E. Iancu and A. Rebhan, *Phys. Lett. B* **523** (2001) 143
- [39] A. Rebhan, arXiv:hep-ph/0301130.
- [40] N. Haque and M. G. Mustafa, arXiv:1007.2076 [hep-ph].

- [41] P. Petreczky, P. Hegde and A. Velytsky [RBC-Bielefeld Collaboration], PoS **LAT2009**, 159 (2009)
- [42] K. -Y. Kim and J. Liao, Nucl. Phys. B **822**, 201 (2009)
- [43] Y. Kim, Y. Matsuo, W. Sim, S. Takeuchi and T. Tsukioka, JHEP **1005**, 038 (2010)
- [44] P. Petreczky, C. Miao and A. Mocsy, Nucl. Phys. A **855**, 125 (2011)
- [45] Á. Mócsy and P. Petreczky, Phys. Rev. D **73**, 074007 (2006)
- [46] Á. Mócsy and P. Petreczky, Phys. Rev. Lett. **99**, 211602 (2007);
- [47] Á. Mócsy and P. Petreczky, Phys. Rev. D **77**, 014501 (2008);
- [48] Á. Mócsy and P. Petreczky, Eur. Phys. J. ST **155**, 101 (2008)
- [49] P. Petreczky, J. Phys. G **37**, 094009 (2010)
- [50] P. Petreczky and K. Petrov, Phys. Rev. D **70**, 054503 (2004)
- [51] O. Kaczmarek *et al.*, Phys. Lett. B **543**, 41 (2002)
- [52] see e.g. Y. Hatta and K. Fukushima, arXiv:hep-ph/0311267, and references therein.
- [53] S. Digal, S. Fortunato and P. Petreczky, Phys. Rev. D **68**, 034008 (2003)
- [54] O. Kaczmarek and F. Zantow, Phys. Rev. D **71**, 114510 (2005)
- [55] P. Petreczky, Eur. Phys. J. C **43**, 51 (2005)
- [56] A. Bazavov, P. Petreczky and A. Velytsky, arXiv:0904.1748 [hep-ph].
- [57] A. Bazavov, P. Petreczky and A. Velytsky, Phys. Rev. D **78**, 114026 (2008)
- [58] N. Brambilla *et al.*, Phys. Rev. D **82**, 074019 (2010)
- [59] M. Cheng *et al.*, Phys. Rev. D **78**, 034506 (2008)
- [60] F. Karsch, M. Oevers and P. Petreczky, Phys. Lett. B **442**, 291 (1998)
- [61] A. Cucchieri, F. Karsch and P. Petreczky, Phys. Lett. B **497**, 80 (2001)
- [62] A. Cucchieri, F. Karsch and P. Petreczky, Phys. Rev. D **64**, 036001 (2001)
- [63] S. Ejiri *et al.*, Phys. Rev. D **80**, 094505 (2009)
- [64] Y. Aoki, *et al.*, Nature **443**, 675 (2006)
- [65] R.D. Pisarski and F. Wilczek, Phys. Rev. D **49**, 338 (1984)
- [66] M. Cheng *et al.*, Eur. Phys. J. C **71**, 1564 (2011)
- [67] O. Kaczmarek *et al.*, Phys. Rev. D **83**, 014504 (2011)
- [68] J. Engels, S. Holtmann, T. Mendes and T. Schulze, Phys. Lett. B **492**, 219 (2000).
- [69] D. Toussaint, Phys. Rev. D **55**, 362 (1997).
- [70] J. Engels and T. Mendes, Nucl. Phys. B **572**, 289 (2000).
- [71] J. Engels, S. Holtmann, T. Mendes and T. Schulze, Phys. Lett. B **514**, 299 (2001).
- [72] M. Asakawa, T. Hatsuda and Y. Nakahara, Prog. Part. Nucl. Phys. **46**, 459 (2001)
- [73] S. Datta *et al.*, Nucl. Phys. Proc. Suppl. **119**, 487 (2003)
- [74] S. Datta, *et al.*, Phys. Rev. D **69**, 094507 (2004)
- [75] T. Umeda, K. Nomura and H. Matsufuru, Eur. Phys. J. C **39S1**, 9 (2005)
- [76] M. Asakawa and T. Hatsuda, Phys. Rev. Lett. **92**, 012001 (2004)
- [77] A. Jakovác *et al.*, Phys. Rev. D **75**, 014506 (2007)
- [78] S. Datta *et al.*, AIP Conf. Proc. **842**, 35 (2006)
- [79] G. Aarts *et al.*, Phys. Rev. D **76**, 094513 (2007)
- [80] F. Karsch, *et al.*, Phys. Rev. D **68**, 014504 (2003) [arXiv:hep-lat/0303017].
- [81] T. Umeda, Phys. Rev. D **75**, 094502 (2007)
- [82] P. Petreczky and D. Teaney, Phys. Rev. D **73**, 014508 (2006)
- [83] P. Petreczky, Eur. Phys. J. C **62**, 85 (2009)
- [84] G. Aarts and J. M. Martinez Resco, Nucl. Phys. B **726** (2005) 93
- [85] S. Mukherjee, Nucl. Phys. A **820** (2009) 283C
- [86] I. Wetzorke, F. Karsch, E. Laermann, P. Petreczky and S. Stickan, Nucl. Phys. Proc. Suppl. **106**, 510 (2002)
- [87] F. Karsch *et al.*, Phys. Lett. B **530**, 147 (2002);
- [88] F. Karsch *et al.*, Nucl. Phys. A **715**, 701 (2003)
- [89] M. Asakawa, T. Hatsuda and Y. Nakahara, Nucl. Phys. A **715**, 863 (2003)
- [90] H. -T. Ding *et al.*, Phys. Rev. D **83**, 034504 (2011)